Leveraging bile solubilization of poorly water-soluble drugs by rational polymer selection

Jonas Schlauersbach[1,#], Simon Hanio[1,#], Bettina Lenz[1],
Sahithya P. B. Vemulapalli[2], Christian Griesinger[2], Ann-Christin Pöppler[3],
Cornelius Harlacher[4], Bruno Galli[4], Lorenz Meinel[1,5,*]

[1] Institute for Pharmacy and Food Chemistry, University of Wuerzburg, Am Hubland, DE-97074 Wuerzburg, Germany

[2] Max Planck Institute for Biophysical Chemistry, Am Faßberg 11, DE-37077 Goettingen, Germany

[3] Institute of Organic Chemistry, University of Wuerzburg, Am Hubland, DE-97074 Wuerzburg, Germany

[4] Novartis Pharma AG, Lichtstrasse 35, CH-4056 Basel, Switzerland

[5] Helmholtz Institute for RNA-based Infection Biology (HIRI), Josef-Schneider-Straße 2/D15, DE-97080 Wuerzburg, Germany

[#]both authors contributed equally to the work

Keywords: polymer drug interaction; flux; bile salt; simulated intestinal fluid; colloid

*Corresponding author: Prof. Dr. Dr. Lorenz Meinel, Institute for Pharmacy and Food Chemistry, University of Wuerzburg, Am Hubland, DE-97074 Wuerzburg, Germany, E-Mail: lorenz.meinel@uni-wuerzburg.de

Abstract: Poorly water-soluble drugs frequently solubilize into bile colloids and this natural mechanism is key for efficient bioavailability. We tested the impact of pharmaceutical polymers on this solubilization interplay using proton nuclear magnetic resonance spectroscopy, dynamic light scattering, and by assessing the flux across model membranes. Eudragit E, Soluplus, and a therapeutically used model polymer, Colesevelam, impacted the bile-colloidal geometry and molecular interaction. These polymer-induced changes reduced the flux of poorly water-soluble and bile interacting drugs (Perphenazine, Imatinib) but did not impact the flux of bile non-interacting Metoprolol. Non-bile interacting polymers (Kollidon VA 64, HPMC-AS) neither impacted the flux of colloid-interacting nor colloid-non-interacting drugs. These insights into the drug substance/polymer/bile colloid interplay potentially point toward a practical optimization parameter steering formulations to efficient bile-solubilization by rational polymer selection.

Introduction

Long-lasting supersaturating systems and/or strategies increasing dissolution rates address pharmaceutical challenges of **p**oorly **w**ater-**s**oluble **d**rugs (**PWSD**) [1], including salt design [2-7], nanoparticles [8, 9] and, **a**morphous **s**olid **d**ispersions (**ASD**) [10, 11] among other approaches [12-17] to obtain reproducible and adequate **p**harmaco**k**inetics (**PK**). Polymer excipients used for drug formulation were traditionally referred to as "inert" [18-20] in spite of a role in e.g. drug transporter inhibition [21], allergic reactions [22], or physicochemical interactions [23]. Other reports highlighted the impact of these excipients on the natural solubilization systems [24, 25] and the current manuscript is within this context. Bile salts (including **t**auro**c**holate – **TC**), phospholipids (including **l**ecithin – **L**), cholesterol, and lipids pour out of the common bile duct into the duodenum and are largely reabsorbed in the ileum [26]. The resulting aqueous **t**auro**c**holate and **l**ecithin **mi**xed **m**icelles (denoted **TC/L MIM**) form the natural solubilization systems for poorly water-soluble vitamins and PWSDs [27-30]. For example, MIM solubilization is key for vitamin K absorption [31], e.g. reflected by the fact that healthy neonates readily absorb orally given vitamin K [29], while absorption occurs to a lesser extent in neonates with an obstructed bile duct/cholestasis [32]. For the most part, the focus of publications on pharmaceutical polymers detail aspects of drug dissolution and the impact on drug permeation across the gut epithelial barrier [33-35]. Selected examples along these lines are the use of **H**ydroxy**p**ropyl **m**ethyl**c**ellulose **a**cetate **s**uccinate (**HPMC-AS**) increasing the bioavailability of a PWSD [36], while the amino methacrylate copolymer Eudragit E, though increasing the apparent drug solubility *in vitro*, resulted in delayed and reduced systemic availability as compared to control without polymer [37]. We hypothesize that reduced bioavailability for PWSDs in the presence of polymer excipients such as Eudragit E is in part due to polymer induced changes in the MIM colloidal structure, thereby impacting MIM solubilization of drugs. We used **Fa**sted **S**tate **S**imulated **I**ntestinal **F**luid (**FaSSIF**) as a model biological fluid containing TC/L MIM as seen in bile [24, 27, 38]. We characterized the impact of polymers (modified polyallylamine (Colesevelam), Eudragit E, polyvinyl caprolactam–polyvinyl acetate–polyethylene glycol graft copolymer (Soluplus), vinylpyrrolidone-vinyl acetate copolymer (Kollidon VA 64), and HPMC-AS) on the molecular interaction within TC/L MIM by **^{1}H n**uclear **m**agnetic **r**esonance (**^{1}H NMR**) and on changes on colloidal geometries by **d**ynamic **l**ight **s**cattering (**DLS**). Both methods combined provided the necessary granularity to assess geometries by hydrodynamic radii and molecular interaction by ^{1}H NMR analysis. Throughout the manuscript we are using the terms "MIM interacting polymers" or "MIM *non*-interacting polymers" to indicate the interaction of *polymers* with TC/L MIM. Colesevelam was selected as a model polymer used therapeutically due to its bile acid/TC binding ability [39]. Eudragit E is a glazing agent used for taste masking

in many pharmaceutical formulations [40, 41] and in ASD formulations [42]. Soluplus has also been used for ASDs [43, 44]. Kollidon VA 64 is a dry binder, granulating agent, and film forming agent [45], HPMC-AS an enteric coating material [46], and both polymers are used as solid dispersion carrier, or precipitation inhibitor [47]. Furthermore, we compared the polymer impact on the solubilization and flux across an artificial membrane for the poorly water soluble drugs Perphenazine and Imatinib with the water soluble and well permeable drug Metoprolol [48]. Throughout the manuscript we are using the terms "MIM interacting drugs" or "MIM *non*-interacting drugs" to indicate the interaction of *drugs* with TC/L MIM. The flux across these artifical membranes has been previously correlated to bioavailability [49-51]. The outcome of our experiments led to a preliminary decision tree by which drug substances are firstly categorized in those for which interaction with bile colloids is critical or not. Depending on this initial classification, secondly classes of pharmaceutical polymers are proposed for TC/L MIM solubilizing drug substances or for drug substance, which do not or marginally interact with TC/L MIM.

Materials and Methods

Materials

Hydroxypropyl methylcellulose acetate succinate (HPMC-AS, grade LF) was obtained from Shin-Etsu Chemical Co Ltd. (Tokyo, Japan). Eudragit E PO was kindly provided by Evonik Nutrition and Care GmbH (Essen, Germany). Kollidon VA 64 and Soluplus were kindly provided by BASF SE (Ludwigshafen, Germany). Colesevelam was purchased from BOCSCI Inc. (New York, USA). Deionized, purified water (Millipore water) was generated by in-house Millipore purification system from Merck KGaA (Darmstadt, Germany). Hexadeuteriodimethyl sulfoxide (DMSO-d_6, 99.8% D) was purchased from Euriso-top (Saarbrücken, Germany) and deuterated water (D_2O, 99.9% D) from Deutero GmbH (Kastellaun, Germany). Deuterated water (D_2O, 99.9% D) containing 0.05% 3-(trimethylsilyl)propionic-2,2,3,3-d_4 sodium salt (TSP-d_4), 40% sodium deuteroxide in deuterated water (NaOD, 99% D), 35% deuterium chloride in deuterated water (DCl, 99% D), sodium chloride (99%), monobasic sodium phosphate monohydrate (99%), D-α-Tocopherol polyethylene glycol 1000 succinate (Vitamin E TPGS), Perphenazine (99%), Metoprolol (99%) were purchased from Sigma-Aldrich (Schnelldorf, Germany). Imatinib free base was kindly provided by Novartis Pharma AG (Basel, Switzerland). Coaxial insert tubes and NMR tubes (5 mm, clear and amber glass) were purchased from Norell, Inc. (Landisville, PA USA). FaSSIF (FeSSIF/FaSSGF) powder was purchased from biorelevant.com Ltd. (London, UK). All other standard chemicals and laboratory consumables, if not stated otherwise, were purchased from either VWR International GmbH (Ismaning, Germany) or Sigma-Aldrich.

Methods

Dynamic Light Scattering

DLS was assessed by a DelsaNanoHC particle analyzer (Beckman Coulter Inc., Brea, California) with a backscattering angle of 165°. Modified **p**hosphate **b**uffered **s**aline pH 6.5 (**PBS**) and FaSSIF-V1 (hereinafter referred to as TC/L in PBS) with a concentration of 3 mmol/l TC and 0.75 mmol/l L were prepared according to the manufacturer's protocol (biorelevant.com). The respective polymer amount in medium (PBS or TC/L in PBS) was shaken for 2 h at 25 °C, 750 rpm on a Thermomixer F1.5 (Eppendorf AG, Hamburg, Germany). Unfiltered samples were measured in disposable 1.5 ml UV-Cuvettes (Brand GmbH & Co. KG, Wertheim, Germany) in triplicate with an accumulation of 70 scans in each run. Data was analyzed using the CUMULANT method. The Z-Average particle size was evaluated with a refractive index of 1.333 as determined for TC/L in PBS by an Abbe refractometer (Carl Zeiss AG, Oberkochen, Germany). The hydrodynamic diameter was adjusted by the dynamic viscosities of the respective solutions as read with a rolling-ball viscometer LOVIS 2000 M using capillary LOVIS 1.8 equipped with a steel ball at an inclination angle of 70° (diameter 1.5 mm, steel 1.4125, density 7.66 g/cm^3, Anton Paar GmbH, Graz, Austria). The temperature was set to 298 K for all experiments. Density was determined using an Anton Paar Density Meter DMA 4100 M. Samples with visible particles were excluded from statistical analysis.

^{1}H Nuclear Magnetic Resonance Spectroscopy

For ^{1}H NMR measurements a 0.1 mol/l DMSO-d_6 drug stock solution was prepared. Deuterated water was used for media preparation. Briefly, for pH adjustment in deuterated water a correction factor was used adjusting pD to 6.91 using DCl and NaOD [52]. Perphenazine experiments were carried out under light protection. 1 mmol/l drug solutions were prepared by adding stock solution to the deuterated medium or polymer/medium mixtures, subsequently shaking for 2 h, 25 °C, and 750 rpm on a Thermomixer. ^{1}H NMR spectra were recorded on a Bruker Avance 400 MHz spectrometer (Bruker BioSpin GmbH, Karlsruhe, Germany) operating at 400.13 MHz with a BBI BB-H 5 mm probe head and at a temperature of 300 K. For ^{1}H NMR experiments the acquisition parameters were set to 256 scans with 56 dummy scans for sample equilibration, flip angle of 30°, a broad spectral width of 20.55 ppm to record all possible signals, and transmitter offset of 6.175 ppm. The acquisition time was 3.985 seconds followed by a relaxation delay of 1.0 second with collection of 64 000 data points at a sample spinning frequency of 20 Hz to ensure proper signal resolution (no spinning side bands were observed). The data were processed using TopSpin 4.0.6 (Bruker BioSpin). An exponential line broadening window function of 0.3 Hz was used (no difference in noise was seen at 0.5 Hz, data not shown). Automatic baseline correction and manual phasing were applied. The chemical shifts were referenced to the external standard of 0.05% TSP-d_4 in D_2O filled in a coaxial insert tube. Proton peaks from deuterated solvents such as DMSO-d_6 are denoted DMSO-d_5 which

comprises all isotopomers of DMSO with at least one detectable proton. For ^{1}H **d**iffusion-**o**rdered **s**pectroscop**y** (DOSY) polymers and media compounds were dried (60 °C, 24 h) in a vacuum drier (Heraeus GmbH, Hanau, Germany). Samples in deuterated TC/L in PBS and PBS were prepared in a constantly nitrogen flushed sekuroka glove box (Carl Roth GmbH & Co. KG, Karlsruhe, Germany). Signal assignment was done using ^{13}C, ^{1}H-^{1}H **co**rrelated **s**pectroscop**y** (COSY), and edited ^{1}H-^{13}C **h**eteronuclear **s**ingle **q**uantum **c**oherence (**HSQC**) spectra as described before [24]. DOSY spectra were recorded at 298 K on Bruker Avance Neo 600 MHz spectrometer (Bruker BioSpin) operating at 600.25 MHz for ^{1}H, equipped with a 5 mm TCI cryo probe containing a z-axis gradient coil with a maximum gradient strength of 58.305 G cm^{-1}. A pulse sequence for diffusion measurement using double stimulated echo for convection compensation and longitudinal eddy current delay sequence with bipolar gradient pulses for diffusion and 3 spoil gradients was used (dstebpgp3s) [53, 54]. A series of 16 spectra with a linear gradient ramp from 25 to 70% of the maximum gradient strength were recorded with an eddy current delay of 5 ms and a recycle delay of 5 s. The water (HDO) diffusion coefficients were obtained after data processing by fitting signal intensity at 4.703 ppm using dynamics center 2.6 (Bruker BioSpin) as a function of gradient strength (Eq. 1).

$$I(G) = I_0 \cdot e^{-\gamma^2 \cdot G^2 \cdot \delta^2 \cdot (\Delta - \frac{\delta}{3}) \cdot D} \quad \text{(Eq.1)}$$

Where *I(G)* is the gradient strength dependent signal intensity, I_0 initial signal intensity, γ gyromagnetic ratio of protons (4258 Hz/Gauss), *G* gradient strength, δ gradient length (2 ms), Δ diffusion time (50 ms), and *D* diffusion coefficient. The HDO signal decayed to below 5% of the initial signal intensity.

Flux

A side-by-side diffusion cell (PermeGear Inc., Hellertown, USA) was used (for assay workflow refer to **Figure S1**). The donor and receiver compartments (each with a filling volume of 10 ml) were separated by a regenerated cellulose membrane with an average pore size of 33 nm according to the manufacturer (innoME GmbH, Espelkamp, Germany). The orifice had a diameter of 15 mm resulting in a surface area of 1.77 cm². The five polymers were tested either in TC/L in PBS or in PBS (0.05% and 1%; % means weight per weight unless stated otherwise) and shaken on an orbital shaker Reax 20 for 2 h (Heidolph GmbH, Schwabach, Germany), and then transferred to the donor chamber. Eudragit E was additionally tested at a concentration of 0.01%. The receiver compartment was filled with PBS containing 0.2% Vitamin E TPGS. In all experiments, the maximum concentration in the receiver cell was less than one tenth of the amount added to the donor (sink condition). The temperature was held at 298 K using a Haake Fisons C1 water circulator (Thermo Fisher Scientific Inc., Karlsruhe, Germany) with a DLK 1002 cooling unit (FRYKA GmbH, Esslingen, Germany). The fluids in the cells were

stirred continuously at 500 rpm on a H9-CB-02 stirring apparatus (SES GmbH, Bechenheim, Germany). At the beginning of the diffusion experiment, a 0.1 mol/l drug stock solution in DMSO was added to achieve a nominal starting concentration of 1 mmol/l. The total amount of DMSO never exceeded 1% (v/v). Perphenazine experiments were carried out under light protection. After 5, 15, 30, 60, 120, 180, and 240 minutes aliquots of 100 µl were taken from the receiver medium and replaced with fresh PBS containing 0.2% Vitamin E TPGS. Subsequently, the samples were diluted with 25 µl of **ac**eto**n**itrile (**ACN**) containing 0.1% **t**ri**f**luoro**a**cetic acid (**TFA**), vortexed for at least 30 seconds (VTX-3000L, LMSCO. LTD., Tokyo, Japan), and centrifuged with a MiniSpin centrifuge (Eppendorf) at 13000 rpm for 10 minutes.

High Pressure Liquid Chromatography Analysis

High **P**ressure **L**iquid **C**hromatography (**HPLC**) was used to determine the receiver compartment concentration change over time. The flux in nmol/min·cm² was obtained from the slope of the resulting concentration versus time profile using linear regression per permeated area. The amount of drug in the acceptor increased linearly showing a high coefficient of correlation ($R^2 > 0.996$). Experiments were carried out in triplicate. Samples were analyzed with an Agilent 1260 infinity II HPLC (Agilent Technologies Inc., Waldbronn, Germany) using a Synergi™ 4 µm Hydro-RP18 80 Å 150 x 4.6 mm LC column (Phenomenex LTD, Aschaffenburg, Germany). The device was equipped with a variable wavelength detector (G7114A, Agilent), an automatic vialsampler (G7129C, Agilent), flexible Pump (G7104C, Agilent), and multicolumn oven (G7116A, Agilent). Mobile phase A was 0.1% TFA in Millipore water. Mobile phase B was ACN with 0.1% TFA, flow was set to 1 ml/min, injection volume was 50 µl, and the wavelength of the detector was set to $\lambda = 255$ nm for Perphenazine, $\lambda = 267$ nm for Imatinib, and $\lambda = 275$ nm for Metoprolol. The gradient started at 20% B increasing to 100% within 6 minutes, held for 4 minutes, then back to 20% B within 1 minute, and held for 4 minutes. Quantification was done by calibration curves (**Figure S2**).

Statistical Analysis

DLS and Metoprolol flux were statistically evaluated by one-way ANOVA followed by *post hoc* Dunnett's test for pairwise comparison with the control group. For flux, pairwise comparisons of all groups were done by *post hoc* Tukey test. Homogeneity of variance was tested by a Levene-test. A double-sided Grubb's test was used for outlier testing and excluded data points are always mentioned in the respective figure legend. Data was considered statistically significant at $p \leq 0.05$. OriginPro 2017 (OriginLab Corporation, Northampton, MA, USA) was used for statistical analysis.

Results

Drug interaction with taurocholate/lecithin mixed micelles

We analyzed the interaction of Perphenazine and Metoprolol with TC/L MIM by ^{1}H NMR spectroscopy. In the ^{1}H NMR spectrum, the TC/L signals appeared in the range 0.7 to 5.3 ppm which is in agreement with the previously reported measurement (**Figure 1A, S3, S4**) [24]. TC H12, H7, H3, H21, H19, H18, and L H4 proton signals shifted to lower ppm in the presence of Perphenazine thereby indicating interaction of the drug substance with TC/L MIM. This was also reflected by Perphenazine's aryl-proton signals shifting to lower ppm in the presence of TC/L MIM (**Figure 1B**, **S4, S7**). In contrast, no chemical shift of TC/L signals were observed in the presence of Metoprolol including Metoprolol's aryl-proton resonances (**Figure 1A, 1C**), orthogonally confirming previous reports [55].

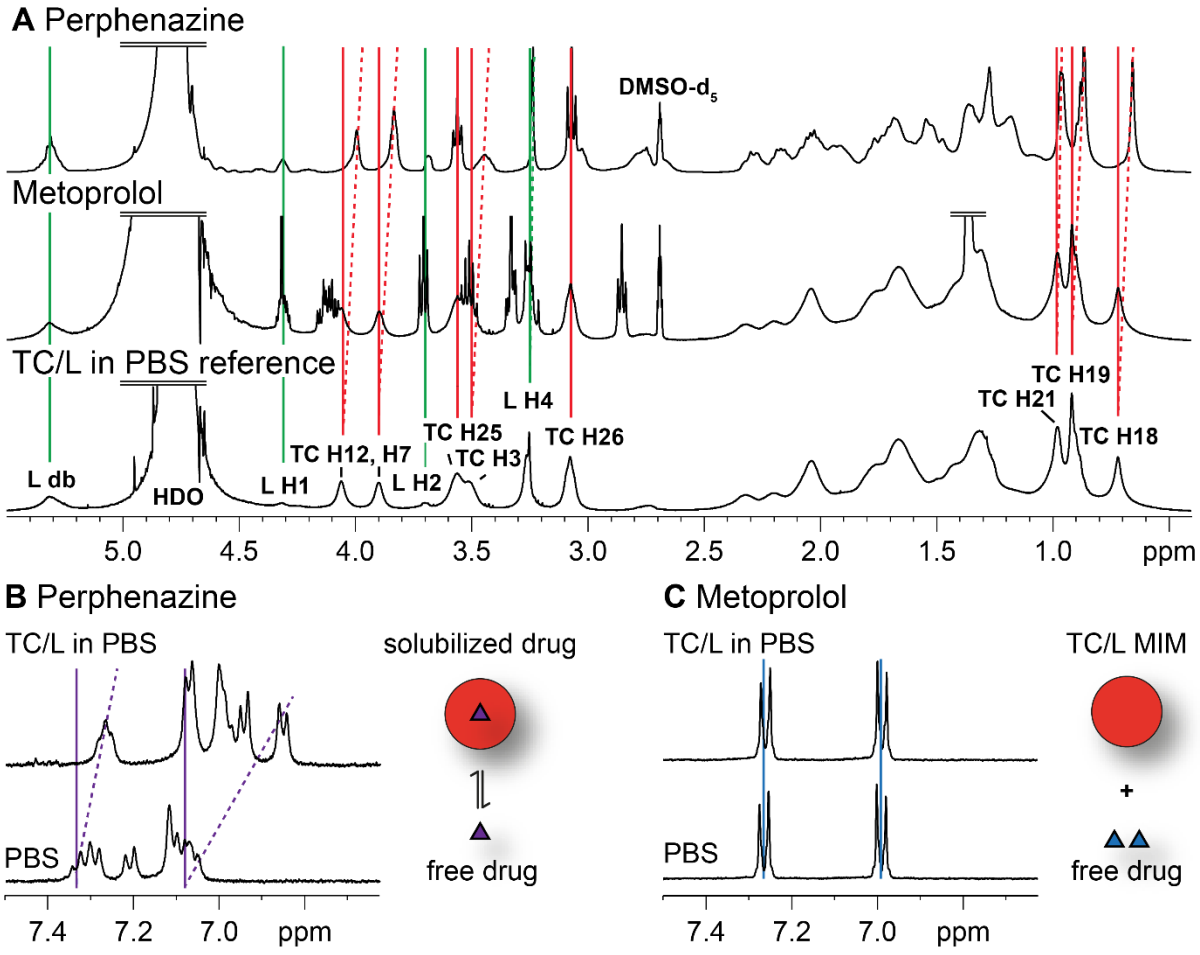

Figure 1: ^{1}H NMR spectra of Perphenazine – interacting with TC/L MIM - and Metoprolol - not interacting with TC/L MIM. (A) ^{1}H NMR spectra of TC/L in PBS as reference (bottom; green and red lines for L and TC signals, respectively), TC/L in PBS with Metoprolol (center), and TC/L in PBS with Perphenazine (top). ^{1}H NMR aryl-proton excerpt of (B) Perphenazine, and (C) Metoprolol in TC/L in PBS (top), and in PBS (bottom) including cartoons abstracting findings for the TC/L MIM interaction with (B) Perphenazine (purple triangle) and absence of interaction of (C) Metoprolol (blue triangles). Signal shifts are indicated by dotted lines.

We refer to analogous studies for Imatinib, which is integrated into the assessment of drug substance/polymer/TC/L MIM interactions (*vide infra*) [24]. Complete ^{1}H NMR spectra, chemical structures, and the approach of aryl-proton spectra interpretation is outlined in the supplementary information (**Figure S3-8**).

Polymer interaction with taurocholate/lecithin mixed micelles

We characterized the polymers in PBS and their impact on TC/L in PBS concerning colloidal size change and molecular interaction by DLS and ^{1}H NMR spectroscopy, respectively. The hydrodynamic diameter of TC/L MIM was 73.0 ± 0.9 nm (**Figure 2A**).

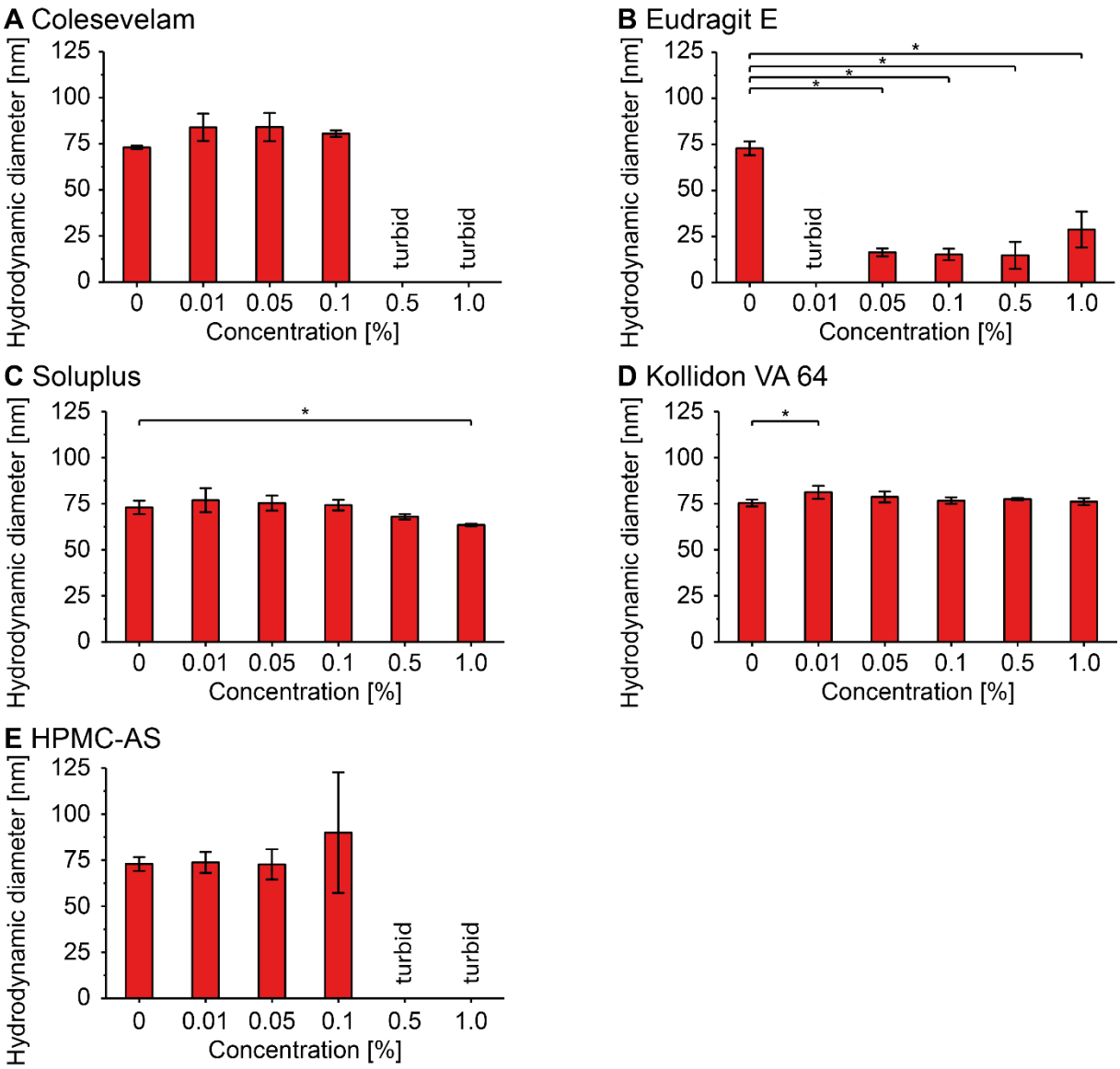

Figure 2: Hydrodynamic diameter of colloids in TC/L in PBS with (A) Colesevelam, (B) Eudragit E, (C) Soluplus, (D) Kollidon VA 64, and (E) HPMC-AS at concentrations as indicated measured by DLS. DLS outcome from turbid samples is qualitatively reported. Data shown as mean ± **s**tandard **d**eviation (**SD**), ANOVA considering $p \leq 0.05$ as statistically significant followed by Dunnett's *post-hoc* for pairwise comparison to the 0% polymer group (significant differences are shown by asterisks).

Colesevelam at 0.5 and 1% resulted in visually turbid samples (**Figure 2A**). Eudragit E - insoluble at 0.01% in TC/L in PBS – was visually turbid (**Figure 2B**). At ≥ 0.05% Eudragit E, particles were formed with 15 to 30 nm in diameter. Soluplus did not impact the size of the TC/L MIM other than at 1% (**Figure 2C**) nor did Kollidon VA 64 (**Figure 2D**), or HPMC-AS (**Figure 2E**). DLS results of the polymers in PBS are detailed in the supplementary information (**Figure S9, Table S1-3**). Furthermore, we analyzed polymers in TC/L in PBS and in PBS by ^{1}H NMR spectroscopy. No Colesevelam signals were seen in PBS and the TC/L signal intensities decreased in presence of this TC binding polymer (**Figure 3A**). Eudragit E reduced the intensity of the TC/L signals with signal broadening observed for TC protons in the range 0.5 to 1.2 ppm (**Figure 3B**). TC signals from 3.8 to 4.2 ppm were no longer observed, while L H4 at 3.25 ppm and TC H26 at 3.1 ppm remained detectable. Soluplus effects in TC/L in PBS were comparable to Eudragit E (**Figure 3C**). In contrast, neither the presence of Kollidon VA 64 (**Figure 3D**) nor HPMC-AS (**Figure 3E**) shifted TC/L signals.

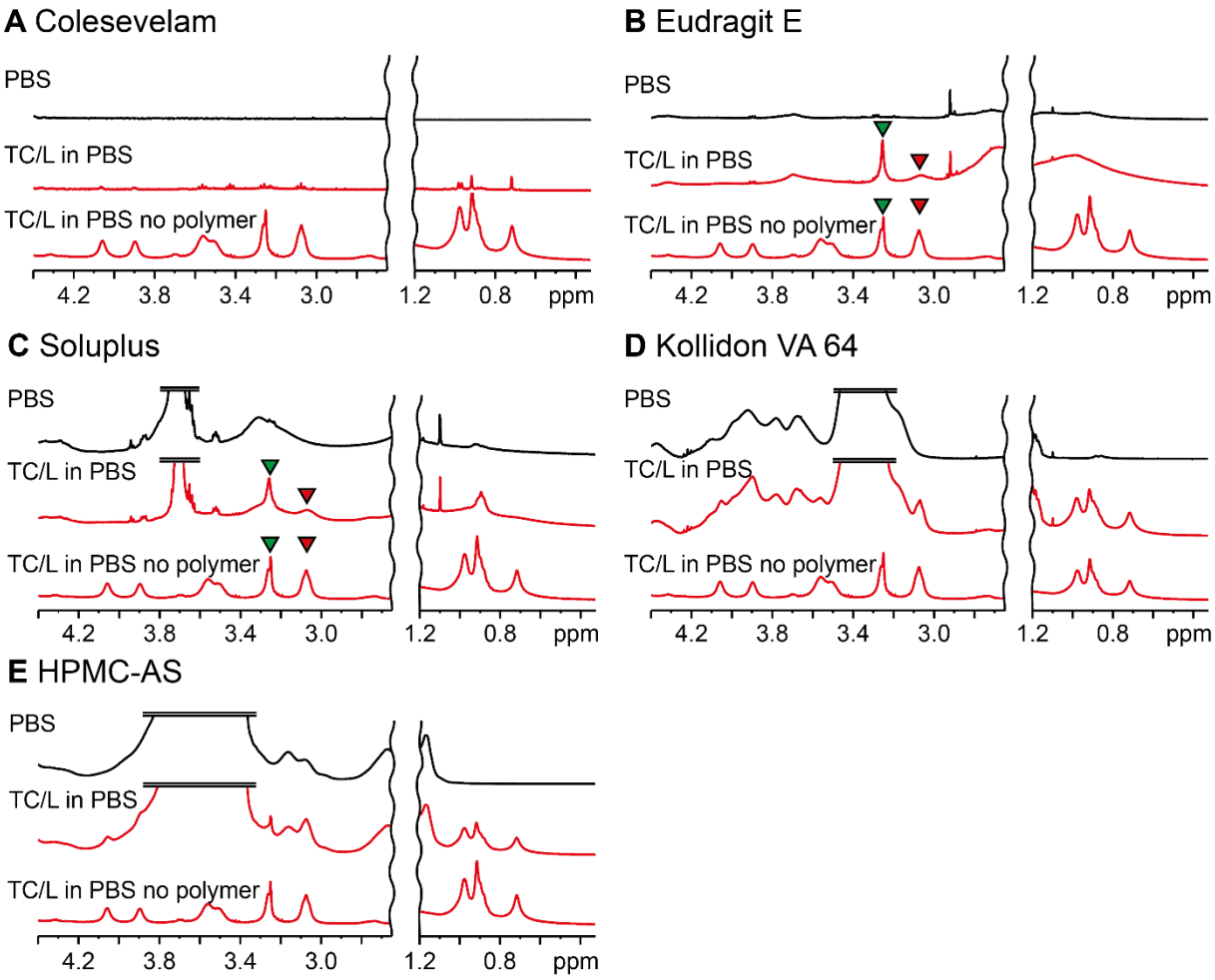

Figure 3: Extracts from ^{1}H NMR spectra of 1% (A) Colesevelam, (B) Eudragit E, (C) Soluplus, (D) Kollidon VA 64, and (E) HPMC-AS in PBS (top, black), in TC/L in PBS (center, red), and for comparison and identical across panels in TC/L in PBS without polymer as reference (bottom, red). L H4 (green triangle pointing at 3.25 ppm) and TC H26 (red triangle pointing at 3.1 ppm) are highlighted for the assessment of polymer/TC/L MIM interaction, which was seen for (A) Colesevelam, (B) Eudragit E, and (C) Soluplus but not (D) Kollidon VA 64, nor (E) HPMC-AS.

Concentration dependent polymer effects on TC/L signals, polymer signals in PBS, chemical structures, and complete ^{1}H NMR spectra are detailed in the supplementary information (**Figure S10-S22**).

Impact of polymers on Perphenazine flux across and aryl-proton signals in presence and in absence of taurocholate/lecithin mixed micelles

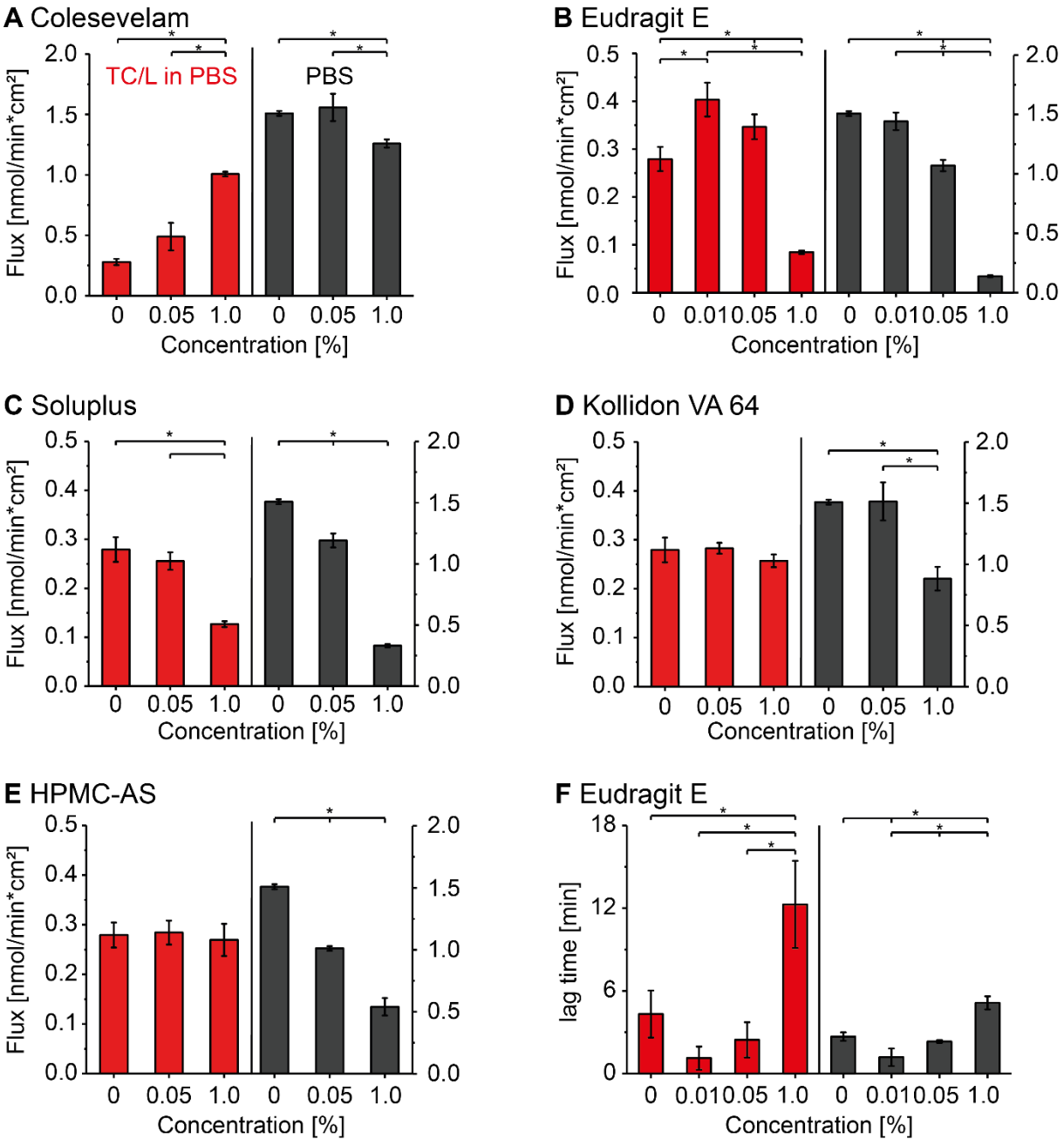

Figure 4: Perphenazine flux with (A) Colesevelam, (B) Eudragit E, (C) Soluplus, (D) Kollidon VA 64, and (E) HPMC-AS in TC/L in PBS (red) and in PBS (black) at concentrations as indicated. (F) Lag time with Eudragit E in TC/L in PBS (red) and in PBS (black) at concentrations as indicated. The left ordinate refers to data recorded in TC/L in PBS (red bars), the right ordinate to in PBS (black bars). Data at 0% polymer concentration are identical for all flux panels and given for comparison. Data shown as mean ± SD, ANOVA considering $p \leq 0.05$ as statistically significant followed by Tukey *post-hoc* test for pairwise comparison (significant differences are shown by asterisks).

Subsequently, we focused on the impact of the polymers on Perphenazine's flux in TC/L in PBS and in PBS across regenerated cellulose membranes, which were previously used in correlation studies of flux and bioavailability [49-51]. DLS studies indicated that aggregates did not permeate across the cellulose membrane (nominal pore size 33 nm according to the manufacturer), including aggregates bellow 33 nm as seen for Eudragit E (data not shown). Perphenazine's flux was reduced by 82% when solubilized into TC/L MIM as compared to PBS (**Figure 4**). Colesevelam increased the Perphenazine flux in TC/L in PBS in a concentration dependent manner contrasting observations in PBS (**Figure 4A**). Increased Perphenazine flux was recorded at low Eudragit E concentrations (0.01 and 0.05%) in TC/L in PBS, but was reduced at 1% Eudragit E in TC/L in PBS and at all Eudragit E concentrations in PBS (**Figure 4B**). Soluplus resulted in a concentration dependent flux decrease in both TC/L in PBS and in PBS (**Figure 4C**). The flux did not change in TC/L in PBS when Kollidon VA 64 was added, but decreased in PBS at 1% Kollidon VA 64 (**Figure 4D**). Similarly, HPMC-AS did not reduce the flux in TC/L in PBS, contrasting findings in PBS (**Figure 4E**). The lag time of Perphenazine increased at 1% Eudragit E in TC/L in PBS and in PBS as compared to without polymer (**Figure 4F**). Colesevelam reduced the lag time as a function of the polymer concentration in TC/L in PBS. 1% HPMC-AS increased the lag time in TC/L in PBS and in PBS (**Figure S44**). In addition to flux experiments, we analyzed Perphenazine's aryl-proton signals in TC/L in PBS in the presence of the polymers detailing the molecular interactions likely driving the flux effects. Signals broadened and shifted to higher ppm at 1% Colesevelam as compared to Perphenazine in TC/L in PBS, while in PBS signal intensity decreased and signals broadened (**Figure 5A**). The aryl-proton signals shifted to higher ppm with increasing Eudragit E concentration, decreased in intensity, and disappeared at 1% Eudragit E in TC/L in PBS (**Figure 5B**). In PBS, aryl-proton signals shifted with increasing Eudragit E concentration to lower ppm and broadened along with intensity decrease. Soluplus decreased Perphenazine's signal intensity with increasing polymer concentration in TC/L in PBS and in PBS (**Figure 5C**). Additionally, broadening of the signals was observed. Kollidon VA 64 had no impact on the aryl-proton signals and only a slight shift to higher ppm was observed in TC/L in PBS (**Figure 5D**). In PBS signals sharpened and intensity increased as compared to Perphenazine in PBS. Perphenazine's aryl-proton signals broadened and shifted to higher ppm at 1% HPMC-AS with unchanged signal intensity in TC/L in PBS (**Figure 5E**). In PBS signals broadened and intensity decreased as a function of HPMC-AS concentration. Our interpretation of the aryl-proton spectra is outlined (**Figure S8**) and complete ^{1}H NMR spectra are provided in the supplementary information (**Figure S23-S27**).

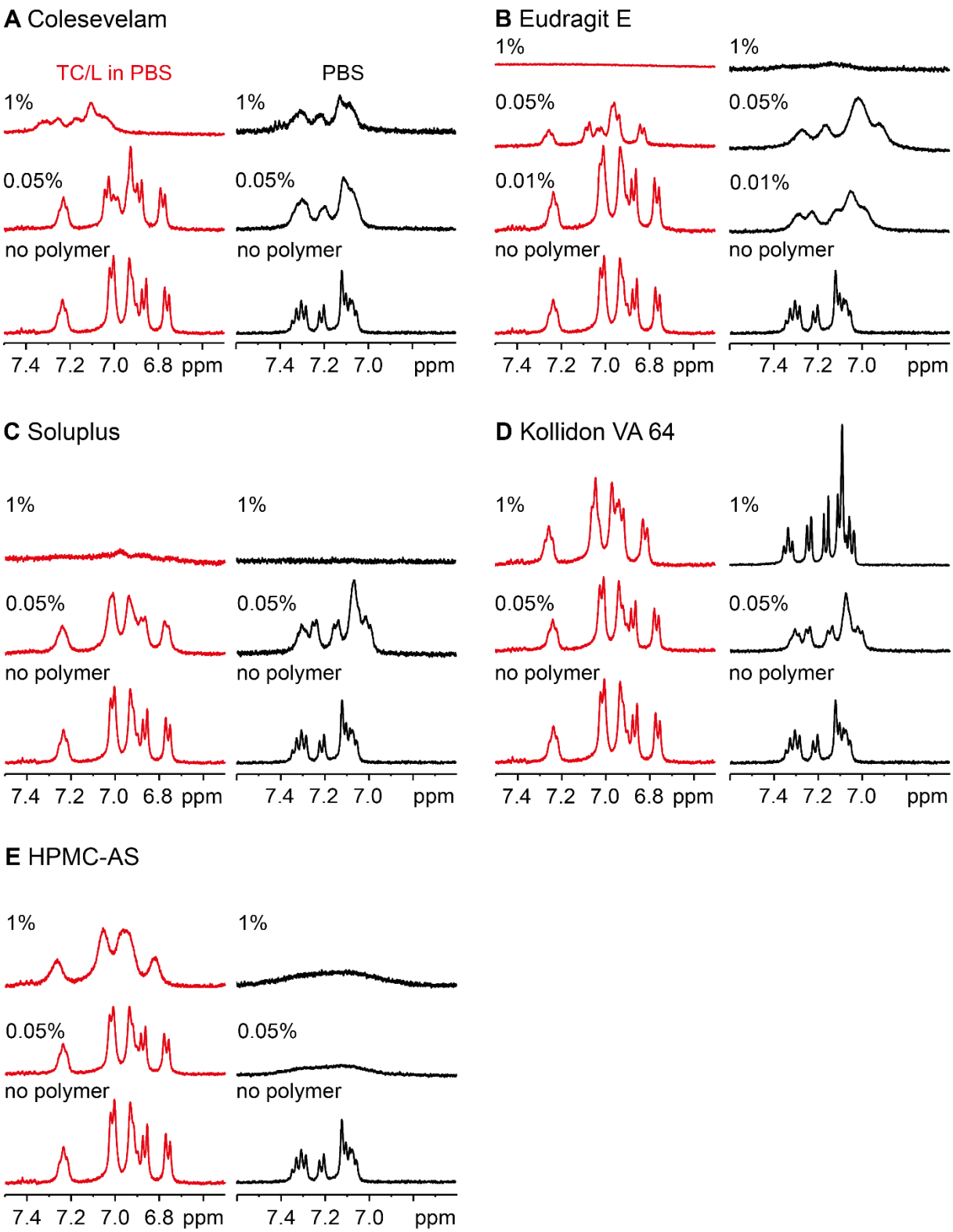

Figure 5: ^{1}H NMR excerpt of Perphenazine aryl-protons in TC/L in PBS (red) and in PBS (black) with (A) Colesevelam, (B) Eudragit E, (C) Soluplus, (D) Kollidon VA 64, and (E) HPMC-AS at concentrations as indicated. The reference spectrum of Perphenazine recorded in TC/L in PBS (red) and in PBS (black) is identical across panels and for comparison (no polymer).

Impact of polymers on Imatinib flux across and aryl-proton signals in presence and in absence of taurocholate/lecithin mixed micelles

In addition to Perphenazine, we analyzed the impact of the polymers on Imatinib's flux in TC/L in PBS and in PBS. Imatinib's interaction with TC/L MIM was previously described [24]. Imatinib's flux was reduced in TC/L in PBS as compared to in PBS (**Figure 6**).

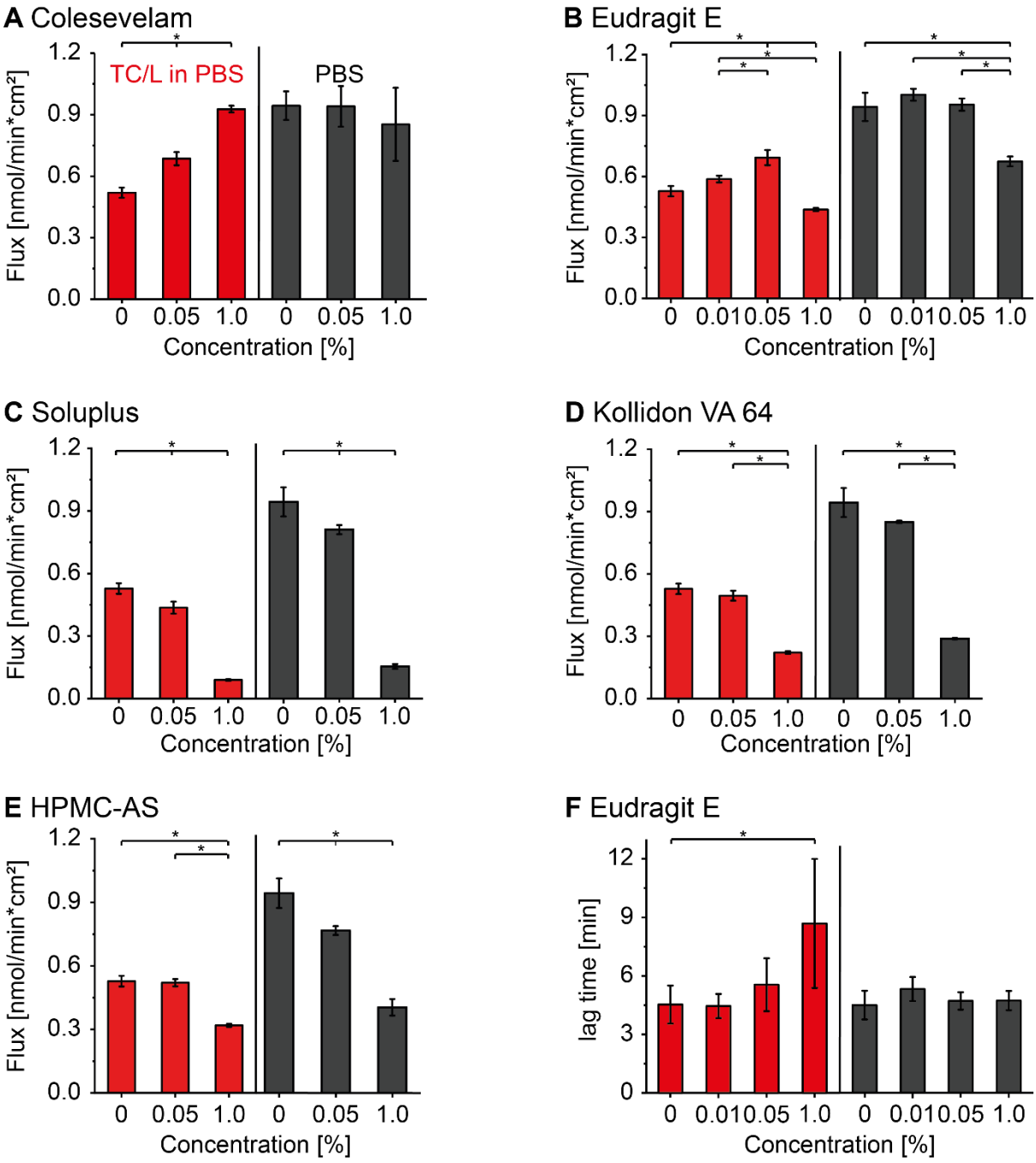

Figure 6: Imatinib flux with (A) Colesevelam, (B) Eudragit E, (C) Soluplus, (D) Kollidon VA 64, and (E) HPMC-AS in TC/L in PBS (red) and in PBS (black) at concentrations as indicated. (F) Lag time with Eudragit E in TC/L in PBS (red) and in PBS (black) at concentrations as indicated. The left ordinate refers to data recorded in TC/L in PBS (red bars), the right ordinate to in PBS (black bars). Data at 0% polymer concentration are identical for all panels and given for comparison. Data shown as mean ± SD, ANOVA considering $p \leq 0.05$ as statistically significant followed by Tukey *post-hoc* test for pairwise comparison (significant differences are shown by asterisks).

Adding Colesevelam to TC/L in PBS increased the flux as a function of Colesevelam concentration (**Figure 6A**). At 1% Colesevelam, the flux in TC/L in PBS was within the range of flux in PBS.

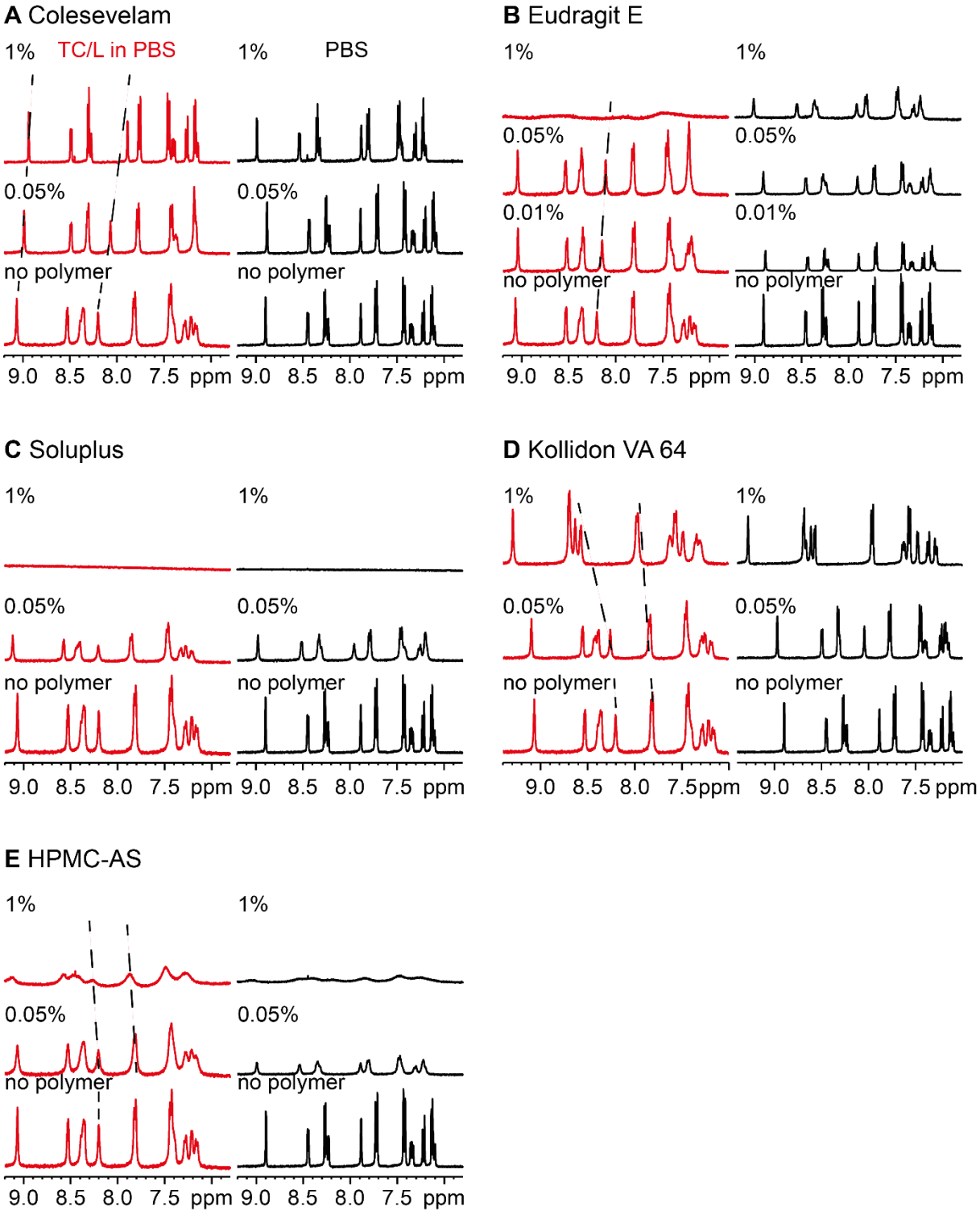

Figure 7: ^{1}H NMR excerpt of Imatinib aryl-protons in TC/L in PBS (red) and in PBS (black) with (A) Colesevelam, (B) Eudragit E, (C) Soluplus, (D) Kollidon VA 64, and (E) HPMC-AS at concentrations as indicated. The reference spectrum of Imatinib recorded in TC/L in PBS (red) and in PBS (black) is identical across panels and for comparison (no polymer). Signal shifts are indicated by dotted lines.

At 0.05% Eudragit E, the flux increased in TC/L in PBS and decreased at 1% Eudragit E in TC/L in PBS and in PBS (**Figure 6B**). Soluplus reduced the flux in a concentration dependent manner in both, in TC/L in PBS and in PBS (**Figure 6C**). Kollidon VA 64 reduced Imatinib flux at 1% in TC/L in PBS (**Figure 6D**), as well as in PBS throughout the entire concentration range (**Figure 6D**). HPMC-AS also reduced the Imatinib flux at 1% in TC/L in PBS and in PBS (**Figure 6E**). The lag time was significantly increased in presence of 1% Eudragit E in TC/L in PBS but not in PBS (**Figure 6F**) and the other polymers had no impact on the lag time (**Figure S45**). We also analyzed Imatinib's aryl-proton signals in the presence of the polymers in TC/L in PBS and in PBS. Imatinib aryl-proton signals in TC/L in PBS sharpened and shifted at 1% Colesevelam as compared to Imatinib without polymer (**Figure 7A**). At 1% Colesevelam in PBS, Imatinib aryl-proton signals shifted to higher ppm as compared to without polymer. Eudragit E caused signal shifts and at 1% the signals broadened and their intensity decreased in TC/L in PBS and in PBS (**Figure 7B**). Broad signals were recorded at 1% Eudragit E in TC/L in PBS. With increasing Soluplus concentration the signal intensity decreased continuously and shifting to higher ppm. At 1% Soluplus all signals disappeared in TC/L in PBS and in PBS (**Figure 7C**). In the presence of Kollidon VA 64 signals shifted to higher ppm values as a function of concentration in TC/L in PBS and in PBS (**Figure 7D**). Increasing HPMC-AS concentration resulted in signal broadening along with intensity decrease in TC/L in PBS and in PBS (**Figure 7E**). Broad signals were recorded at 1% HPMC-AS in PBS. All complete ^{1}H NMR spectra are detailed in the supplementary information (**Figure S28-S32**).

Impact of polymers on Metoprolol flux across and aryl-proton signals in presence and in absence of taurocholate/lecithin mixed micelles

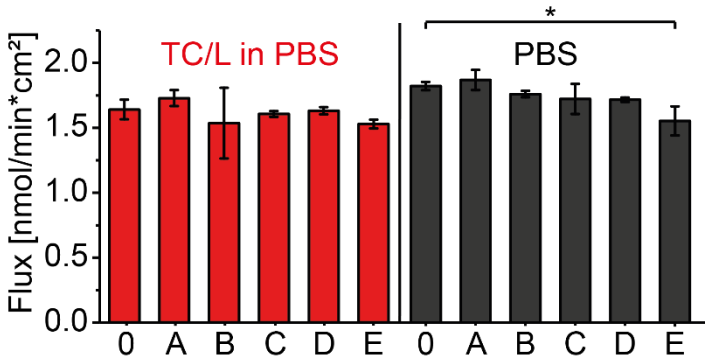

Figure 8: Metoprolol flux (0) in absence of polymer, with 1% (A) Colesevelam, (B) Eudragit E, (C) Soluplus, (D) Kollidon VA 64, and (E) HPMC-AS in TC/L in PBS (red) and in PBS (black). Data shown as mean ± SD, ANOVA considering $p \leq 0.05$ as statistically significant followed by Dunnett's *post-hoc* for pairwise comparison with the 0% polymer group (significant differences are shown by asterisks).

The last studied drug was Metoprolol. The flux was reduced in TC/L in PBS as compared to in PBS (**Figure 8**). None of the polymers had an impact on Metoprolol flux in TC/L in PBS. Significant flux reduction was observed

for 1% HPMC-AS in PBS as compared to in PBS. Except for Soluplus, Metoprolol aryl-proton signals were not impacted by the polymers in TC/L in PBS and in PBS (**Figure S33, S34**).

Diffusion coefficient of water in taurocholate/lecithin in PBS and the impact of polymer supplementation

At last we determined diffusion coefficients of HDO in the presence of the polymers to assess the impact of diffusion on flux. The HDO diffusivity - in TC/L in PBS with Perphenazine - was $2.79 \cdot 10^{-9}$ m²/s (**Figure S35**) and was not impacted by the presence of any of the polymers at any concentration (**Table S4**).

4. Discussion

Colesevelam, Eudragit E, and Soluplus impacted TC/L MIM structure (referred to as "MIM interacting polymers") and Kollidon VA 64 or HPMC-AS did not ("MIM *non*-interacting polymers"; **Figure 2, 3**). These MIM *non*-interacting polymers formed supramolecular aggregates existing next to the TC/L MIM (**Figure S9**). Perphenazine was effectively solubilized into TC/L MIM (**Figure 1**). Similarly, Imatinib was integrated into TC/L MIM as previously described [24]. In the presence of MIM interacting polymers the molecular interaction of these drugs within the MIM and the resulting free drug fraction were significantly impacted as compared to polymer-free conditions (**Figure 4**, **6**). Perphenazine shifts observed in presence of Colesevelam – used as a positive control among our polymers - were particularly striking, arguably reflecting the therapeutic use of this polymer in contrast to the other polymers which are used as excipients. In contrast, water soluble and well permeable Metoprolol did not interact with TC/L MIM (**Figure 1**) and its flux across membranes was barely or not affected by the MIM interacting polymers (**Figure 8**).

We hypothesized that MIM interacting polymers impact the molecular dynamics of TC/L MIM differently, as compared to MIM *non*-interacting polymers, and that these differences impact the flux of PWSDs across membranes. To address this hypothesis, we screened polymer concentrations from 0.01 to 1% - concentrations with possible clinical significance (**Section S6**) [41, 56-59]. We started analyzing the impact of Colesevelam- an ion exchanging polymer used for bile salt binding [39] – on MIM structure and MIM molecular assembly hypothesizing and confirming that the polymer particularly impacted negatively charged TC (**Figure S3, S10, S12**). Colesevelam reduced the ^{1}H NMR signal intensity of TC and L in a Colesevelam-concentration dependent manner (**Figure 3, S12**), indicating that Colesevelam pushes TC/L from MIM into insoluble TC/L/Colesevelam particles and further reflected by the presence of aggregates (**Figure 2**). Consequently, we expected less TC/L MIM in presence of Colesevelam, hence reduced effects on crystallization inhibition, solubility or dissolution rate of PWSDs, respectively, and as previously suggested [60-62]. Similarly, Eudragit E – frequently used in numerous

formulations [41] - impacted the TC/L micellar system in a concentration dependent manner. Low Eudragit E concentrations resulted in *insoluble* aggregates containing TC/L with non-detectable ^{1}H NMR signals for L but still detectable TC signals suggesting efficient entrapment of L and to a lesser extent TC within these Eudragit E aggregates (**Figure 2, S14**). Furthermore, the lag time was significantly increased at 1% Eudragit E for both, Perphenazine and Imatinib (**Figure 4, 6**), whereas the other polymers had marginal lag time effects (**Figures S44, S45**). This may point to slower exchange kinetics of drug substance from Eudragit E structures as compared to the other polymers. Hence, Eudragit E's ability of integrating TC and L into its aggregates may critically jeopardize the solubilization of PWSD, findings which have previously suggested by others [63-65] and possibly causal to previously observed reductions in bioavailability of PWSD in presence of Eudragit E [37, 66-68]. At higher concentrations, these Eudragit E aggregates were not observed and *soluble* Eudragit E/TC/L MIM were formed. The ^{1}H NMR TC/L signals broadened and decreased in signal intensity indicating aggregates with high molecular density and the colloids were smaller for the Eudragit E/TC/L MIM as compared to TC/L MIM (**Figure 2, 3, S8, S9**). This data confirmed previous studies reporting Eudragit E dynamics leading to either insoluble or soluble supramolecular aggregates as a function of polymer concentration [27, 58]. Similar to Eudragit E, Soluplus - an excipient enhancing the bioavailability of some PWSDs [68, 69] – interacted with TC/L MIM but in contrast to Eudragit E did not show polymer concentration effects on the formation of insoluble aggregates and soluble colloids (**Figure 3**). In alignment with previous reports, Soluplus impacted the size of TC/L MIM (**Figure 2, S8, S9**) [70, 71]. Temperature effects in this range are particularly pronounced for Soluplus with a cloud point between 25 – 37 °C [72]. Kollidon VA 64 and similarly HMPC-AS at a concentration of up to 0.1% had no impact on TC/L MIM molecular structure or colloidal hydrodynamic diameters and our data indicated that pure polymer aggregates existed separate of the TC/L MIM (**Figure 2, 3**). HPMC-AS at a concentration of 0.5% and 1% generated insoluble aggregates in TC/L in PBS and in PBS resulting in turbid solutions (**Figure 2, S9**). Based on ^{1}H NMR we observed a coexistence of TC/L MIM and HPMC-AS supramolecular aggregates (**Figure 3, S20**). Soluplus had a minor impact on hydrodynamic diameters in DLS (**Figure 2**) but interacted with TC/L MIM (^{1}H NMR; **Figure 3, S25**). Future studies may further detail the resulting colloidal structures, particularly whether these structures are supramolecular or ionic. In summary, we categorized our polymers as MIM interacting (Colesevelam, Eudragit E, and Soluplus) or MIM *non*-interacting polymers (Kollidon VA 64, HPMC-AS).

We then proceeded to study the impact of either polymer category on the solubilization of drugs into TC/L MIM, and detailed the resulting supramolecular interaction of polymer, TC/L MIM, and flux. In analogy to the polymers (*vide supra*), we categorized drugs into those which interact with TC/L MIM and others that do not. Perphenazine

and Imatinib interacted with TC/L MIM [24] whereas Metoprolol did not (**Figure 1**). Drug integration into the TC/L MIM - as observed for Perphenazine and Imatinib - reduced the flux across cellulose membranes (**Figure 4, 6**). These effects depended on the TC/L concentration with higher TC/L concentrations (simulating fed state) further reducing the flux (**Figure S36-S38**) and as described before [73]. Furthermore, flux depended on drug substance solubility which is why we selected a concentration (1 mmol/l) resulting in kinetically stable solutions throughout all experimental durations (**Figure S38-S43**). The flux was tested across cellulose membranes, which had previously been correlated to drug substance bioavailability [49-51]. This has been also shown for lipophilic membranes [74, 75] but we selected cellulose membranes here to focus mostly on size exclusion. We confirmed efficient size exclusion by the absence of visible particles or DLS determined structures (data not shown). Thereby, the rate limiting step in our experiments were the events in the donor chamber and not in the diffusion layer (membrane and aqueous boundary layers) for all polymers as seen with Metoprolol (**Figure 8**). In addition, we excluded possible obstruction effects by the polymers in the donor compartment as demonstrated by comparable water (HDO) diffusion in solution among the experimental conditions (**Figure S35**) [76, 77]. In conclusion, the absence of polymer obstruction effects on diffusion (**Figure S35**), absence of polymer impact on the diffusion across the diffusion layer as concluded from unaltered flux and lag time for Metoprolol (**Figure 8, S46**), we assigned the differences in flux as discussed below (**Figure 4, 6**) and lag times observed for Perphenazine and Imatinib (**Figure S44, S45**) directly to drug release phenomena from supramolecular structures including colloids being present in the donor chamber.

Starting off these findings, we studied the impact of MIM interacting polymers and MIM *non*-interacting polymers on these drugs in presence of TC/L MIM. This resulted in the differentiation of three distinct patterns. One pattern was seen with (i) Colesevelam or Eudragit E (at low concentrations) reducing the available TC/L for solubilization and consequently increasing the free drug fraction (^{1}H NMR signal shift) and flux of the MIM interacting drugs Perphenazine and Imatinib (**Figure 4-7**). An increase in free drug fraction of Perphenazine in presence of Colesevelam – as seen by higher flux (**Figure 4A**) – might also be reflected by the increased diffusion coefficient (**Table S5**). In contrast, the MIM *non*-interacting drug Metoprolol was not impacted by the presence of these polymers (**Figure 8, S33, and S34**). Metaphorically, both polymers push the drugs out of the TC/L MIM and into solution – obviously, a finding only relevant for drugs integrating into TC/L MIM. This might reduce bioavailability of drugs and fat-soluble vitamins relying on bile related solubilization [32, 60-62]. A contrasting pattern (ii) was observed for Eudragit E at higher concentration and Soluplus at any concentration. Both reduced the free drug fraction (^{1}H NMR signals shifted and decreased in intensity) and consequently the flux of MIM

interacting but not MIM *non*-interacting drugs, respectively. This was in line with the formation of new colloidal structures combining all components, the polymer, the drug, and the TC/L MIM (**Figure 4-8**). Signals for Perphenazine (**Figure 5**) and Imatinib (**Figure 7**) shifted to higher ppm or lower ppm as compared to without polymer, phenomena detailed for guest-host cyclodextrin complexes before linking shifts to higher and lower ppm to hydrophilic and hydrophobic interaction, respectively [78-80]. Lastly, a third (iii) pattern was observed for the polymers which did not substantially interact with TC/L MIM but formed separate aggregates (Kollidon VA 64 and HPMC-AS; **Figure 3**). These polymers did not (Perphenazine) or marginally (Imatinib) impact the flux of MIM interacting (**Figure 4, 6, Section S8**) or MIM *non*-interacting drugs (Metoprolol; **Figure 8**). For example, in spite of unaltered flux - hence unaltered free drug fraction - aryl-proton signal broadening of Perphenazine was observed at 1% as compared to 0.05% HPMC-AS (**Figure 5**). Because of concurrent Perphenazine flux reduction with HPMC-AS in PBS but not in TC/L in PBS, we attribute this signal broadening to drug-polymer but not MIM-polymer interaction, respectively, assuming that the MIM *non*-interacting character of the polymers does not change in presence of drug. This interpretation would also link to previous reports, reporting improved drug bioavailability with these MIM *non*-interacting polymers [50, 81, 82]. The three polymer patterns are summarized below (**Figure 9**) and potentially introduce a further optimization parameter in formulation design.

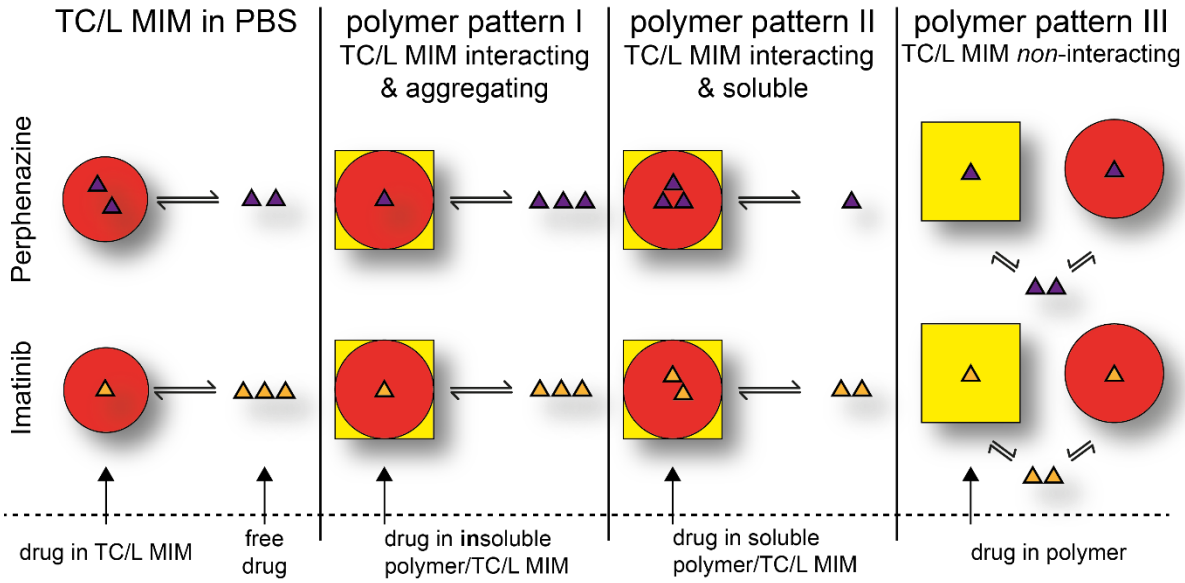

Figure 9: Illustration of interaction patterns seen for polymers (yellow squares) with TC/L MIM (red circle) with respective drugs. The cartoon abstracts Perphenazine's (purple triangle) and Imatinib's (orange triangle) relative partition into different structures formed by polymer and TC/L MIM as seen from the flux experiments.

5. Conclusion

Efficient solubilization by bile colloids is important for the bioavailability of many PWSD, hydrophobic vitamins or other essential components [25, 32, 50]. Hence, supporting this mechanism with properly selected polymers for

formulation might offer advantages and lead to better performing medication. Along these lines, we identified three patterns by which polymers impacted the molecular assembly and geometry of bile colloids and we linked these patterns to different flux rates of PWSD. Flux rates were previously correlated to bioavailability [49-51]. For those who wish to translate these findings into pharmaceutical application, we propose starting with the assessment whether a PWSD is solubilized by bile or not. If not (as for Metoprolol), polymer selection is rather uncritical even if the polymers affect TC/L molecular assembly and structure. However, if the PWSD interacts with the TC/L (as for Perphenazine and Imatinib), polymer selection is critical. Hence, this strategy integrates into polymer selection for maximizing the molecularly dissolved drug substance at resorption sites and extends these known strategies by taking polymer effects on bile solubilization into account. This and other exciting formulation strategies may unfold at this point. We summarize this approach in a preliminary decision tree (**Figure 10**).

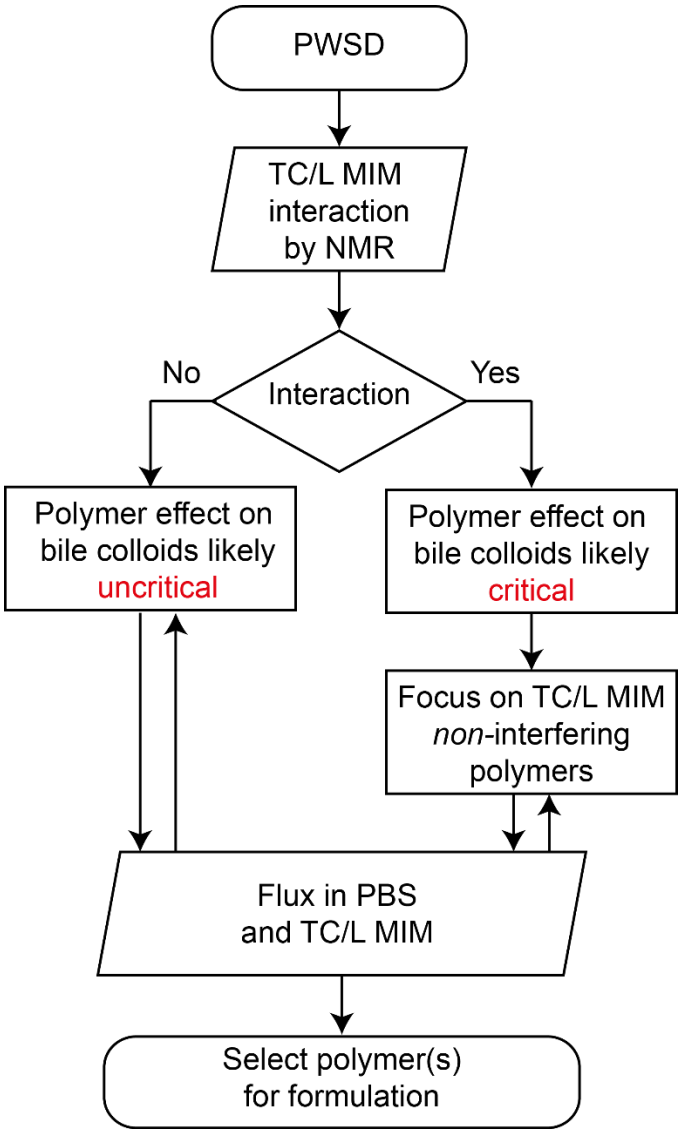

Figure 10: Preliminary decision tree for polymer selection. We classify Colesevelam, Eudragit E, and Soluplus as critical polymers in terms of TC/L MIM interaction, in contrast to uncritical polymers Kollidon VA 64 and HPMC-AS.

Possibly, future algorithms may allow prediction including performances in other fluids, e.g. fed state simulating gastrointestinal fluids and potentially biological aspirates.

Acknowledgements

We gratefully acknowledge the financial support by Novartis Pharma AG for JS. BG and CH are full time associated of Novartis and declare a possible conflict of interest. We also acknowledge the kind support by the Max Planck Gesellschaft. We would like to thank Christopher Heidenreich and Alexandra Mony for their great technical assistance.

References

[1] T. Jiang, N. Han, B. Zhao, Y. Xie, S. Wang, Enhanced dissolution rate and oral bioavailability of simvastatin nanocrystal prepared by sonoprecipitation, Drug Dev. Ind. Pharm., 38 (2012) 1230-1239.
[2] M. Reggane, J. Wiest, M. Saedtler, C. Harlacher, M. Gutmann, S.H. Zottnick, P. Piechon, I. Dix, K. Muller-Buschbaum, U. Holzgrabe, L. Meinel, B. Galli, Bioinspired co-crystals of Imatinib providing enhanced kinetic solubility, Eur. J. Pharm. Biopharm., 128 (2018) 290-299.
[3] A. Balk, U. Holzgrabe, L. Meinel, 'Pro et contra' ionic liquid drugs - Challenges and opportunities for pharmaceutical translation, Eur. J. Pharm. Biopharm., 94 (2015) 291-304.
[4] A. Balk, J. Wiest, T. Widmer, B. Galli, U. Holzgrabe, L. Meinel, Transformation of acidic poorly water soluble drugs into ionic liquids, Eur. J. Pharm. Biopharm., 94 (2015) 73-82.
[5] A. Balk, T. Widmer, J. Wiest, H. Bruhn, J.C. Rybak, P. Matthes, K. Muller-Buschbaum, A. Sakalis, T. Luhmann, J. Berghausen, U. Holzgrabe, B. Galli, L. Meinel, Ionic liquid versus prodrug strategy to address formulation challenges, Pharm. Res., 32 (2015) 2154-2167.
[6] J. Wiest, M. Saedtler, A. Balk, B. Merget, T. Widmer, H. Bruhn, M. Raccuglia, E. Walid, F. Picard, H. Stopper, W. Dekant, T. Luhmann, C. Sotriffer, B. Galli, U. Holzgrabe, L. Meinel, Mapping the pharmaceutical design space by amorphous ionic liquid strategies, J. Control. Release., 268 (2017) 314-322.
[7] P. Güntzel, K. Schilling, S. Hanio, J. Schlauersbach, C. Schollmayer, L. Meinel, U. Holzgrabe, Bioinspired Ion Pairs Transforming Papaverine into a Protic Ionic Liquid and Salts, ACS Omega, 5 (2020) 19202-19209.
[8] D. Horn, J. Rieger, Organic Nanoparticles in the Aqueous Phase—Theory, Experiment, and Use, Angew. Chem. Int. Ed., 40 (2001).
[9] E.M. Merisko-Liversidge, G.G. Liversidge, Drug nanoparticles: formulating poorly water-soluble compounds, Toxicol. Pathol., 36 (2008) 43-48.
[10] K. Six, T. Daems, J. de Hoon, A. Van Hecken, M. Depre, M.P. Bouche, P. Prinsen, G. Verreck, J. Peeters, M.E. Brewster, G. Van den Mooter, Clinical study of solid dispersions of itraconazole prepared by hot-stage extrusion, Eur. J. Pharm. Sci., 24 (2005) 179-186.
[11] A.C. Pöppler, M.M. Lubtow, J. Schlauersbach, J. Wiest, L. Meinel, R. Luxenhofer, Loading-Dependent Structural Model of Polymeric Micelles Encapsulating Curcumin by Solid-State NMR Spectroscopy, Angew. Chem. Int. Ed. Engl., 58 (2019) 18540-18546.
[12] C.J. Porter, C.W. Pouton, J.F. Cuine, W.N. Charman, Enhancing intestinal drug solubilisation using lipid-based delivery systems, Adv. Drug Deliv. Rev., 60 (2008) 673-691.
[13] D. Singh, N. Bedi, A.K. Tiwary, Enhancing solubility of poorly aqueous soluble drugs: critical appraisal of techniques, J. Pharm. Investig., 48 (2017) 509-526.
[14] J. Bevernage, J. Brouwers, M.E. Brewster, P. Augustijns, Evaluation of gastrointestinal drug supersaturation and precipitation: strategies and issues, Int. J. Pharm., 453 (2013) 25-35.
[15] M. Rodriguez-Aller, D. Guillarme, J.L. Veuthey, R. Gurny, Strategies for formulating and delivering poorly water-soluble drugs, J. Drug Deliv. Sci. Technol., 30 (2015) 342-351.
[16] J. Wiest, J. Kehrein, M. Saedtler, K. Schilling, E. Cataldi, C.A. Sotriffer, U. Holzgrabe, T. Rasmussen, B. Bottcher, M. Cronin-Golomb, M. Lehmann, N. Jung, M. Windbergs, L. Meinel, Controlling Supramolecular Structures of Drugs by Light, Mol. Pharm., (2020).
[17] A. Gamboa, N. Schussler, E. Soto-Bustamante, P. Romero-Hasler, L. Meinel, J.O. Morales, Delivery of ionizable hydrophilic drugs based on pharmaceutical formulation of ion pairs and ionic liquids, Eur. J. Pharm. Biopharm., 156 (2020) 203-218.
[18] P. Crowley, L.G. Martini, Drug-excipient interactions, Pharm. Technol., 4 (2001) 7-12.

[19] J. Pottel, D. Armstrong, L. Zou, A. Fekete, X.P. Huang, H. Torosyan, D. Bednarczyk, S. Whitebread, B. Bhhatarai, G. Liang, H. Jin, S.N. Ghaemi, S. Slocum, K.V. Lukacs, J.J. Irwin, E.L. Berg, K.M. Giacomini, B.L. Roth, B.K. Shoichet, L. Urban, The activities of drug inactive ingredients on biological targets, Science, 369 (2020) 403-413.
[20] L. Golightly, S. Smolinske, M. Bennett, E.r. Sutherland, B. Rumack, Pharmaceutical excipients. Adverse effects associated with inactive ingredients in drug products (Part I), Med. Toxicol. Adv. Drug., 3(2) (1988 Mar-Apr) 128-165.
[21] M. Werle, Natural and synthetic polymers as inhibitors of drug efflux pumps, Pharm. Res., 25 (2008) 500-511.
[22] D. Reker, S.M. Blum, C. Steiger, K.E. Anger, J.M. Sommer, J. Fanikos, G. Traverso, "Inactive" ingredients in oral medications, Sci. Transl. Med., 11 (2019).
[23] E. Borbas, P. Tozser, K. Tsinman, O. Tsinman, K. Takacs-Novak, G. Volgyi, B. Sinko, Z.K. Nagy, Effect of Formulation Additives on Drug Transport through Size-Exclusion Membranes, Mol. Pharm., 15 (2018) 3308-3317.
[24] J. Wiest, M. Saedtler, B. Böttcher, M. Grüne, M. Reggane, B. Galli, U. Holzgrabe, L. Meinel, Geometrical and Structural Dynamics of Imatinib within Biorelevant Colloids, Mol. Pharm., 15 (2018) 4470-4480.
[25] K. Sugano, M. Kataoka, C. Mathews Cda, S. Yamashita, Prediction of food effect by bile micelles on oral drug absorption considering free fraction in intestinal fluid, Eur. J. Pharm. Sci., 40 (2010) 118-124.
[26] A.F. Hofmann, The enterohepatic circulation of bile acids in mammals: form and functions, Front. Biosci. , 14 (2009) 2584-2598.
[27] D. Riethorst, P. Baatsen, C. Remijn, A. Mitra, J. Tack, J. Brouwers, P. Augustijns, An In-Depth View into Human Intestinal Fluid Colloids: Intersubject Variability in Relation to Composition, Mol. Pharm., 13 (2016) 3484-3493.
[28] D. Riethorst, R. Mols, G. Duchateau, J. Tack, J. Brouwers, P. Augustijns, Characterization of Human Duodenal Fluids in Fasted and Fed State Conditions, J. Pharm. Sci., 105 (2016) 673-681.
[29] G. Schubiger, C. Stocker, O. Banziger, B. Laubscher, H. Zimmermann, Oral vitamin K1 prophylaxis for newborns with a new mixed-micellar preparation of phylloquinone: 3 years experience in Switzerland, Eur. J. Pediatr., 158 (1999) 599-602.
[30] P. Augustijns, B. Wuyts, B. Hens, P. Annaert, J. Butler, J. Brouwers, A review of drug solubility in human intestinal fluids: implications for the prediction of oral absorption, Eur J Pharm Sci, 57 (2014) 322-332.
[31] M.J. Shearer, Vitamin K in parenteral nutrition, Gastroenterology, 137 (2009) S105-118.
[32] F. Sun, T.C. Jaspers, P.M. van Hasselt, W.E. Hennink, C.F. van Nostrum, A Mixed Micelle Formulation for Oral Delivery of Vitamin K, Pharm. Res., 33 (2016) 2168-2179.
[33] A. Schittny, J. Huwyler, M. Puchkov, Mechanisms of increased bioavailability through amorphous solid dispersions: a review, Drug Deliv., 27 (2020) 110-127.
[34] B. Karolewicz, A review of polymers as multifunctional excipients in drug dosage form technology, Saudi Pharm. J., 24 (2016) 525-536.
[35] H. Liu, L.S. Taylor, K.J. Edgar, The role of polymers in oral bioavailability enhancement; a review, Polymer, 77 (2015) 399-415.
[36] A.M. Stewart, M.E. Grass, T.J. Brodeur, A.K. Goodwin, M.M. Morgen, D.T. Friesen, D.T. Vodak, Impact of Drug-Rich Colloids of Itraconazole and HPMCAS on Membrane Flux in Vitro and Oral Bioavailability in Rats, Mol. Pharm., 14 (2017) 2437-2449.
[37] W. Saal, N. Wyttenbach, J. Alsenz, M. Kuentz, Interactions of dimethylaminoethyl methacrylate copolymer with non-acidic drugs demonstrated high solubilization in vitro and pronounced sustained release in vivo, Eur. J. Pharm. Biopharm., 125 (2018) 68-75.
[38] M. Vogtherr, A. Marx, A.C. Mieden, C. Saal, Investigation of solubilising effects of bile salts on an active pharmaceutical ingredient with unusual pH dependent solubility by NMR spectroscopy, Eur. J. Pharm. Biopharm., 92 (2015) 32-41.
[39] M.H. Davidson, M.A. Dillon, B. Gordon, P. Jones, J. Samuels, S. Weiss, J. Isaacsohn, P. Toth, S.K. Burke, Colesevelam hydrochloride (cholestagel): a new, potent bile acid sequestrant associated with a low incidence of gastrointestinal side effects, Arch. Intern. Med., 159 (1999) 1893-1900.
[40] Evonik Nutrition and Care GmbH, Eudragit Polymers for immediate release. https://healthcare.evonik.com/product/health-care/en/products/pharmaceutical-excipients/immediate-release/, 2020 (accessed 01 April 2020).
[41] Medizinische Medien Informations GmbH, Gelbe Liste. https://www.gelbe-liste.de/, 2020 (accessed 31 March 2020).
[42] S. Onoue, Y. Kojo, Y. Aoki, Y. Kawabata, Y. Yamauchi, S. Yamada, Physicochemical and pharmacokinetic characterization of amorphous solid dispersion of tranilast with enhanced solubility in gastric fluid and improved oral bioavailability, Drug Metab. Pharmacokinet., 27 (2012) 379-387.

[43] BASF SE, Technical information soluplus.
https://documents.basf.com/d4806db3b7c1fd04c2fb8d78c37595a170986618?response-content-disposition=inline, 2019 (accessed 01 April 2020).
[44] M. Linn, E.M. Collnot, D. Djuric, K. Hempel, E. Fabian, K. Kolter, C.M. Lehr, Soluplus(R) as an effective absorption enhancer of poorly soluble drugs in vitro and in vivo, Eur. J. Pharm. Sci., 45 (2012) 336-343.
[45] BASF SE, Technical information Kollidon VA 64.
https://documents.basf.com/54e50e670d2ea311a27b33287436dadc3d8373c1?response-content-disposition=inline, 2019 (accessed 01 April 2020).
[46] Shin-Etsu Chemical Co. Ltd, information about Shin-Etsu AQOAT.
https://www.shinetsupharmausa.com/en/pharma_excipients/Shin_etsu_aquoat/index.pmode, 2020 (accessed 01 April 2020).
[47] F. Tanno, Y. Nishiyama, H. Kokubo, S. Obara, Evaluation of hypromellose acetate succinate (HPMCAS) as a carrier in solid dispersions, Drug Dev. Ind. Pharm., 30 (2004) 9-17.
[48] Y. Yang, P.J. Faustino, D.A. Volpe, C.D. Ellison, R.C. Lyon, L.X. Yu, Biopharmaceutics Classification of Selected β-Blockers: Solubility and Permeability Class Membership, Mol. Pharm., 4 (2007) 608-614.
[49] P. Berben, A. Bauer-Brandl, M. Brandl, B. Faller, G.E. Flaten, A.C. Jacobsen, J. Brouwers, P. Augustijns, Drug permeability profiling using cell-free permeation tools: Overview and applications, Eur. J. Pharm. Sci., 119 (2018) 219-233.
[50] Y. Kawai, Y. Fujii, F. Tabata, J. Ito, Y. Metsugi, A. Kameda, K. Akimoto, M. Takahashi, Profiling and Trend Analysis of Food Effects on Oral Drug Absorption Considering Micelle Interaction and Solubilization by Bile Micelles, Drug Metab. Pharmacokinet., 26 (2011) 180-191.
[51] P. Berben, J. Brouwers, P. Augustijns, The artificial membrane insert system as predictive tool for formulation performance evaluation, Int. J. Pharm., 537 (2018) 22-29.
[52] F.G.K. Baucke, Further Insight into the Dissociation Mechanism of Glass Electrodes. The Response in Heavy Water, J. Phys. Chem. B, 102 (1998) 4835-4841.
[53] A. Jerschow, N. Müller, 3D Diffusion-Ordered TOCSY for Slowly Diffusing Molecules, J. Magn. Reson., 123 (1996) 222-225.
[54] A. Jerschow, N. Müller, Suppression of Convection Artifacts in Stimulated-Echo Diffusion Experiments. Double-Stimulated-Echo Experiments, J. Magn. Reson., 125 (1997) 372-375.
[55] M.P. Grosvenor, J.E. Lofroth, Interaction between bile salts and beta-adrenoceptor antagonists, Pharm. Res., 12 (1995) 682-686.
[56] B. Guthrie, B. Makubate, V. Hernandez-Santiago, T. Dreischulte, The rising tide of polypharmacy and drug-drug interactions: population database analysis 1995-2010, BMC Med., 13 (2015) 74.
[57] C.J. Charlesworth, E. Smit, D.S. Lee, F. Alramadhan, M.C. Odden, Polypharmacy Among Adults Aged 65 Years and Older in the United States: 1988-2010, J. Gerontol. A Biol. Sci. Med. Sci., 70 (2015) 989-995.
[58] C. Schiller, C.P. Fröhlich, T. Giessmann, W. Siegmund, H. Monnikes, N. Hosten, W. Weitschies, Intestinal fluid volumes and transit of dosage forms as assessed by magnetic resonance imaging, Aliment. Pharmacol. Ther., 22 (2005) 971-979.
[59] M. Koziolek, M. Grimm, F. Schneider, P. Jedamzik, M. Sager, J.P. Kuhn, W. Siegmund, W. Weitschies, Navigating the human gastrointestinal tract for oral drug delivery: Uncharted waters and new frontiers, Adv. Drug Deliv. Rev., 101 (2016) 75-88.
[60] V. Bakatselou, R.C. Oppenheim, J.B. Dressman, Solubilization and wetting effects of bile salts on the dissolution of steroids, Pharm. Res., 8 (1991) 1461-1469.
[61] S.D. Mithani, V. Bakatselou, C.N. TenHoor, J.B. Dressman, Estimation of the increase in solubility of drugs as a function of bile salt concentration, Pharm. Res., 13 (1996) 163-167.
[62] J. Chen, L.I. Mosquera-Giraldo, J.D. Ormes, J.D. Higgins, L.S. Taylor, Bile Salts as Crystallization Inhibitors of Supersaturated Solutions of Poorly Water-Soluble Compounds, Cryst. Growth Des., 15 (2015) 2593-2597.
[63] A.T. Serajuddin, P.C. Sheen, D. Mufson, D.F. Bernstein, M.A. Augustine, Physicochemical basis of increased bioavailability of a poorly water-soluble drug following oral administration as organic solutions, J. Pharm. Sci., 77 (1988) 325-329.
[64] K. Hu, S. Cao, F. Hu, J. Feng, Enhanced oral bioavailability of docetaxel by lecithin nanoparticles: preparation, in vitro, and in vivo evaluation, Int. J. Nanomed., 7 (2012) 3537-3545.
[65] B.S. Kumar, R. Saraswathi, K.V. Kumar, S.K. Jha, D.P. Venkates, S.A. Dhanaraj, Development and characterization of lecithin stabilized glibenclamide nanocrystals for enhanced solubility and drug delivery, Drug Deliv., 21 (2014) 173-184.
[66] V.R. Sinha, R. Kumria, Binders for colon specific drug delivery: an in vitro evaluation, Int. J. Pharm., 249 (2002) 23-31.
[67] R.I. Moustafine, A.R. Salachova, E.S. Frolova, V.A. Kemenova, G. Van den Mooter, Interpolyelectrolyte complexes of Eudragit E PO with sodium alginate as potential carriers for colonic drug delivery: monitoring of

structural transformation and composition changes during swellability and release evaluating, Drug Dev. Ind. Pharm., 35 (2009) 1439-1451.
[68] T. Yoshida, I. Kurimoto, H. Umejima, S. Watanabe, K. Sako, A. Kikuchi, Effects of dissolved state of aminoalkyl methacrylate copolymer E/HCl on solubility enhancement effect for poorly water-soluble drugs, Colloid and Polym. Sci., 291 (2012) 1191-1199.
[69] R. Pignatello, R. Corsaro, Polymeric Nanomicelles of Soluplus® as a Strategy for Enhancing the Solubility, Bioavailability and Efficacy of Poorly Soluble Active Compounds, Curr. Nanomed., 9 (2019) 184-197.
[70] J.M.O. Pinto, A.F.C. Rengifo, C. Mendes, A.F. Leao, A.L. Parize, H.K. Stulzer, Understanding the interaction between Soluplus(R) and biorelevant media components, Colloids Surf. B 187 (2020) 110673.
[71] J. Thiry, G. Broze, A. Pestieau, A.S. Tatton, F. Baumans, C. Damblon, F. Krier, B. Evrard, Investigation of a suitable in vitro dissolution test for itraconazole-based solid dispersions, Eur. J. Pharm. Sci., 85 (2016) 94-105.
[72] J.R. Hughey, J.M. Keen, D.A. Miller, K. Kolter, N. Langley, J.W. McGinity, The use of inorganic salts to improve the dissolution characteristics of tablets containing Soluplus(R)-based solid dispersions, Eur. J. Pharm. Sci., 48 (2013) 758-766.
[73] K. Yano, Y. Masaoka, M. Kataoka, S. Sakuma, S. Yamashita, Mechanisms of membrane transport of poorly soluble drugs: role of micelles in oral absorption processes, J. Pharm. Sci., 99 (2010) 1336-1345.
[74] A. Dahan, J.M. Miller, The solubility-permeability interplay and its implications in formulation design and development for poorly soluble drugs, AAPS. J. , 14 (2012) 244-251.
[75] Y.N. Abdiche, D.G. Myszka, Probing the mechanism of drug/lipid membrane interactions using Biacore, Anal. Biochem., 328 (2004) 233-243.
[76] S. Cvijic, J. Parojcic, P. Langguth, Viscosity-mediated negative food effect on oral absorption of poorly-permeable drugs with an absorption window in the proximal intestine: In vitro experimental simulation and computational verification, Eur. J. Pharm. Sci., 61 (2014) 40-53.
[77] P. Gao, P.E. Fagerness, Diffusion in HPMC gels. I. Determination of drug and water diffusivity by pulsed-field-gradient spin-echo NMR, Pharm. Res., 12 (1995) 955-964.
[78] K.W. Eckenroad, G.A. Manley, J.B. Yehl, R.T. Pirnie, T.G. Strein, D. Rovnyak, An Edge Selection Mechanism for Chirally Selective Solubilization of Binaphthyl Atropisomeric Guests by Cholate and Deoxycholate Micelles, Chirality, 28 (2016) 525-533.
[79] C.M. O'Farrell, K.A. Hagan, T.J. Wenzel, Water-Soluble Calix[4]Resorcinarenes as Chiral NMR Solvating Agents for Bicyclic Aromatic Compounds, Chirality, 21 (2009) 911-921.
[80] K.J. Smith, J.D. Wilcox, G.E. Mirick, L.S. Wacker, N.S. Ryan, D.A. Vensel, R. Readling, H.L. Domush, E.P. Amonoo, S.S. Shariff, T.J. Wenzel, Calix[4]arene, calix[4]resorcarene, and cyclodextrin derivatives and their lanthanide complexes as chiral NMR shift reagents, Chirality, 15 Suppl (2003) S150-158.
[81] J.M.O. Pinto, A.F. Leao, M.K. Riekes, M.T. Franca, H.K. Stulzer, HPMCAS as an effective precipitation inhibitor in amorphous solid dispersions of the poorly soluble drug candesartan cilexetil, Carbohydr. Polym., 184 (2018) 199-206.
[82] K. Chmiel, J. Knapik-Kowalczuk, K. Jurkiewicz, W. Sawicki, R. Jachowicz, M. Paluch, A New Method To Identify Physically Stable Concentration of Amorphous Solid Dispersions (I): Case of Flutamide + Kollidon VA64, Mol. Pharm., 14 (2017) 3370-3380.